



VICTORIA UNIVERSITY
MELBOURNE AUSTRALIA

Nonlinear analysis of axially loaded circular concrete-filled stainless steel tubular short columns

This is the Accepted version of the following publication

Patel, Vipulkumar Ishvarbhai, Liang, Qing and Hadi, Muhammad NS (2014)
Nonlinear analysis of axially loaded circular concrete-filled stainless steel
tubular short columns. *Journal of Constructional Steel Research*, 101. 9 - 18.
ISSN 0143-974X

The publisher's official version can be found at
<http://www.sciencedirect.com/science/article/pii/S0143974X1400128X>
Note that access to this version may require subscription.

Downloaded from VU Research Repository <https://vuir.vu.edu.au/30020/>

Nonlinear analysis of axially loaded circular concrete-filled stainless steel tubular short columns

Vipulkumar Ishvarbhai Patel^a, Qing Quan Liang^{b,*}, Muhammad N. S. Hadi^c

^a*Institute of Materials Engineering, Australian Nuclear Science and Technology Organisation, Locked Bag 2001, Kirrawee, NSW 2232, Australia*

^b*College of Engineering and Science, Victoria University, PO Box 14428, Melbourne, VIC 8001, Australia*

^c*School of Civil, Mining and Environmental Engineering, University of Wollongong, Wollongong, NSW 2522, Australia*

ABSTRACT

Experiments show that the ultimate compressive strength of stainless steel is much higher than its tensile strength. The full-range two-stage constitutive model for stainless steels assumes that stainless steels follow the same stress–strain behavior in compression and tension, which may underestimate the compressive strength of stainless steel tubes. This paper presents a fiber element model incorporating the recently developed full-range three-stage stress–strain relationships based on experimentally observed behavior for stainless steels for the nonlinear analysis of circular concrete-filled stainless steel tubular (CFSST) short columns under axial compression. The fiber element model accounts for the concrete confinement effects provided by the stainless steel tube. Comparisons of computer solutions with experimental results published in the literature are made to examine the accuracy of the fiber element model and material constitutive models for stainless steels. Parametric studies are conducted to study the effects of various parameters on the behavior of circular CFSST short columns. A design model based on Liang and Fragomeni's design formula is proposed for

*Corresponding author. Tel.: 61 3 9919 4134.
E-mail address: Qing.Liang@vu.edu.au (Q. Q. Liang)

circular CFSST short columns and validated against results obtained by experiments, fiber element analyses, ACI-318 codes and Eurocode 4. The fiber element model incorporating the three-stage stress–strain relationships for stainless steels is shown to simulate well the axial load–strain behavior of circular CFSST short columns. The proposed design model gives good predictions of the experimental and numerical ultimate axial loads of CFSST columns. It appears that ACI-318 codes and Eurocode 4 significantly underestimate the ultimate axial strengths of CFSST short columns.

Keywords: Concrete-filled steel tubes; Fiber element analysis; Stainless steel; Strength

1. Introduction

The material constitutive models used in the nonlinear inelastic analysis of circular concrete-filled stainless steel tubular (CFSST) short columns could have a crucial influence on the accuracy of the predicted behavior. The two-stage stress–strain model for stainless steels proposed by Rasmussen [1] assumes that the stainless steel follows the same stress–strain curve in tension and compression. This model developed from tension coupon tests may underestimate the ultimate axial strengths of CFSST columns. The three-stage constitutive model for stainless steels proposed by Quach et al. [2] accounts for different behavior of stainless steels in compression and in tension based on experimental observations. The three-stage material model is believed to be a more accurate formulation than the two-stage one. The inversion of the three-stage stress–strain relationships for stainless steels given by Abdella et al. [3] expresses the stress as a function of strain. This gives a convenient implementation of the material laws in numerical models. The three-stage stress–strain model

for stainless steels has not yet been incorporated in numerical techniques for the nonlinear analysis of CFSST columns.

Experimental studies on the behavior of axially loaded circular concrete-filled steel tubular (CFST) short columns have extensively been conducted by researchers [4-7]. However, research studies on circular CFSST short columns under axial loading have been relatively limited. Young and Ellobody [8] conducted tests on the axial strengths of cold-formed high strength square and rectangular CFSST short columns. Their results indicated that the implementation of the material properties of stainless steel obtained from tension coupon tests underestimated the ultimate axial strengths of CFSST columns under axial compression. This is because the strain hardening of stainless steels in compression is much higher than that of stainless steels in tension. Tests on circular CFSST short columns under axial compression were carried out by Lam and Gardner [9]. They investigated the effects of the tube thickness, concrete compressive strength and proof stress on the behavior of CFSST columns under axial loading. Design formulas based on the Continuous Strength Method were proposed for determining the ultimate axial strengths of CFSST short columns. Uy et al. [10] tested circular CFSST columns under axial compression. Both square and circular column sections were tested to study the effects of the tube shape, diameter-to-thickness ratio and concrete compressive strength on the behavior of CFSST columns. They compared various design codes for circular CFSST columns. They reported that existing design codes for composite columns provide conservative predictions of the ultimate strengths of CFSST columns.

Numerical models have been developed to study the behavior of circular CFST short columns under axial loading [11-18]. However, there have been relatively limited numerical studies on the behavior of axially loaded circular CFSST short columns. Nonlinear analysis methods for

composite columns and structures have been reviewed by Ellobody [19]. Ellobody and Young [20] utilized the finite element analysis program ABAQUS to study the behavior of axially loaded rectangular CFSST short columns. They incorporated the measured tensile material properties in the finite element model and assumed the same material properties of stainless steel in compression. Nonlinear finite element analyses of square CFSST short columns using ABAQUS have been undertaken by Tao et al. [21]. The two-stage stress–strain model for stainless steels proposed by Rasmussen [1] was employed in their study. The true stress–strain curves were used in the finite element model. Recently, Hassanein et al. [22] employed the finite element program ABAQUS to study the inelastic behavior of axially loaded circular lean duplex CFSST short columns. The finite element results were verified against test results presented by Uy et al. [10].

In this paper, the inversion of the three-stage stress–strain relationships for stainless steels [2, 3] is incorporated in the fiber element model for simulating the nonlinear inelastic behavior of CFSST short columns under axial compression. The fiber element model accounts for the effects of concrete confinement and high strength concrete. The fiber element analyses are performed to examine the accuracy of different constitutive models for stainless steels. The effects of diameter-to-thickness ratio, concrete compressive strength and stainless steel proof stress on the behavior of circular CFSST short columns are investigated. A design model based on Liang and Fragomeni's formula [16] is proposed for the design of circular CFSST columns and compared with test results and design codes.

2. Nonlinear analysis

2.1. Assumptions

The nonlinear analysis of CFSST columns under axial compression is based on the fiber element method. The following assumptions are made in the fiber element formulation:

- The bond between the stainless steel tube and the concrete core is perfect.
- The passive confinement provided by the stainless steel tube increases the compressive strength and ductility of the concrete core.
- The stress and strain of fibers are uniformly distributed on the cross-section.
- Strain hardening of stainless steels in compression is considered.
- Failure occurs when the concrete fiber strain reaches the maximum axial strain.
- Local buckling of the stainless steel tube is not considered.
- The effects of concrete creep and shrinkage are not considered.

2.2. The fiber element method

The fiber element method is an accurate numerical technique for determining the cross-section behavior of steel-concrete composite columns [14, 15, 23-25]. In the fiber element method, a circular CFSST column cross-section is discretized into fine fiber elements as depicted in Fig. 1. Each fiber element represents a fiber of material running longitudinally along the column and can be assigned either stainless steel or concrete material properties. The fiber stresses are calculated from fiber strains using the material uniaxial stress-strain relationships. Although the discretization of a CFSST column under axial compression is not required, it is a prerequisite for the nonlinear analysis of CFSST short columns under eccentric loading or CFSST slender columns [26, 27]. The present study is part of a research program on the nonlinear analysis of CFSST slender columns so that the composite section is

discretized using the fiber element method. However, the size of fiber elements does not affect the ultimate axial strength and behavior of CFSST short columns.

2.3. Material model for stainless steels

The inversion of the full-range three-stage stress–strain relationships for stainless steels presented by Abdella et al. [3] is based on the equations proposed by Quach et al. [2], which is implemented in the present fiber element model. The three-stage stress–strain curve for stainless steels in compression is shown in Fig. 2. In the first stage ($0 \leq \varepsilon_s \leq \varepsilon_{0.2}$) of the stress–strain curve, the stress is expressed by

$$\sigma_s = \frac{E_0 \varepsilon_s \left[1 + C_1 \left(\frac{\varepsilon_s}{\varepsilon_{0.2}} \right)^{C_2} \right]}{1 + C_3 \left(\frac{\varepsilon_s}{\varepsilon_{0.2}} \right)^{C_4} + C_1 \left(\frac{\varepsilon_s}{\varepsilon_{0.2}} \right)^{C_2}} \quad (1)$$

where σ_s is the stress in a steel fiber, ε_s is the strain in the steel fiber, E_0 is the Young's modulus of stainless steel, $\varepsilon_{0.2}$ is the strain at $\sigma_{0.2}$ and $\sigma_{0.2}$ is the 0.2% proof stress. The strain $\varepsilon_{0.2}$ is calculated by the equation given by Ramberg and Osgood [28] as:

$$\varepsilon_{0.2} = \frac{\sigma_{0.2}}{E_0} + 0.002 \quad (2)$$

In Eq. (1), the positive constants C_1, C_2, C_3 and C_4 are given by

$$C_1 = \frac{\Delta}{C_2 - 1} \quad (3)$$

$$C_2 = 1 + \frac{B_1}{\Delta} \quad (4)$$

$$C_3 = G_0(1 + C_1) \quad (5)$$

$$C_4 = \Delta + G_1 \quad (6)$$

in which

$$\Delta = \frac{1 + \sqrt{1 + 4B_1}}{2} \quad (7)$$

$$B_1 = \frac{G_1 E_{0.2} (n + G_0)}{E_0} \quad (8)$$

$$G_0 = \frac{0.002 E_0}{\sigma_{0.2}} \quad (9)$$

$$G_1 = \frac{\varepsilon_{0.2} E_{0.2} (n - 1)}{\sigma_{0.2}} \quad (10)$$

$$E_{0.2} = \frac{E_0}{1 + 0.002 \left(\frac{n}{e} \right)} \quad (11)$$

where $E_{0.2}$ is the tangent modulus of the stress–strain curve at the 0.2% proof stress, n is the nonlinearity index and e is the non-dimensional proof stress given as:

$$e = \frac{\sigma_{0.2}}{E_0} \quad (12)$$

In the second stage ($\varepsilon_{0.2} < \varepsilon_s \leq \varepsilon_{2.0}$), the stress is expressed by the equation presented by Abdella et al. [3]:

$$\sigma_s = \sigma_{0.2} + \frac{E_{0.2}(\varepsilon_s - \varepsilon_{0.2}) \left[1 + C_5 \left(\frac{\varepsilon_s - \varepsilon_{0.2}}{\varepsilon_{1.0} - \varepsilon_{0.2}} \right)^{C_6} \right]}{1 + C_7 \left(\frac{\varepsilon_s - \varepsilon_{0.2}}{\varepsilon_{1.0} - \varepsilon_{0.2}} \right)^{C_8} + C_5 \left(\frac{\varepsilon_s - \varepsilon_{0.2}}{\varepsilon_{1.0} - \varepsilon_{0.2}} \right)^{C_6}} \quad (13)$$

where $\varepsilon_{1.0}$ is the strain at $\sigma_{1.0}$ and $\sigma_{1.0}$ is the 1.0% proof stress.

The 1.0% proof stress under compression can be calculated by the following equation given by Quach et al. [2]:

$$\sigma_{1.0} = \sigma_{0.2} \left(\frac{0.662}{n} + 1.085 \right) \quad (14)$$

The strain $\varepsilon_{1.0}$ is calculated by [2]:

$$\varepsilon_{1.0} = \frac{\sigma_{1.0} - \sigma_{0.2}}{E_{0.2}} + \left[0.008 + (\sigma_{1.0} - \sigma_{0.2}) \left(\frac{1}{E_0} - \frac{1}{E_{0.2}} \right) \right] + \varepsilon_{0.2} \quad (15)$$

In Eq. (13), C_5 , C_6 , C_7 and C_8 are the positive constants,

$$C_5 = \frac{1}{C_6 - 1} \quad (16)$$

$$C_6 = C_8 + \frac{1}{\ln\left(\frac{\varepsilon_{2.0} - \varepsilon_{0.2}}{\varepsilon_{1.0} - \varepsilon_{0.2}}\right)} \left[\ln(1 + A_2) + \ln\left(\frac{H_0}{H_2}\right) \right] \quad (17)$$

$$C_7 = H_0(1 + C_5) \quad (18)$$

$$C_8 = 1 + H_1 \quad (19)$$

where

$$A_2 = \frac{(n_2 - 1)^2 (H_2 - H_0)}{(1 + n_2 H_0)(1 + n_2 H_2)} \quad (20)$$

$$H_0 = \frac{\left[0.008 + (\sigma_{1.0} - \sigma_{0.2}) \left(\frac{1}{E_0} - \frac{1}{E_{0.2}} \right) \right] E_{0.2}}{\sigma_{1.0} - \sigma_{0.2}} \quad (21)$$

$$H_1 = \frac{(n_2 - 1)(H_0 + 1)}{1 + n_2 H_0} \quad (22)$$

$$H_2 = \frac{E_{0.2} \left(\frac{\varepsilon_{2.0} - \varepsilon_{0.2}}{\varepsilon_{1.0} - \varepsilon_{0.2}} \right)}{\sigma_{2.0} - \sigma_{0.2}} \quad (23)$$

In Eq. (17), $\varepsilon_{2.0}$ is the strain at $\sigma_{2.0}$ and $\sigma_{2.0}$ is the 2.0% proof stress. In Eq. (20), n_2 is given by Quach et al. [2] as

$$n_2 = 6.399 \left(\frac{E_{0.2}}{E_0} \right) \left(\frac{\sigma_{1.0}}{\sigma_{0.2}} \right) + 1.145 \quad (24)$$

The 2.0% proof stress can be calculated by the following equation given by Quach et al. [2]:

$$\sigma_{2.0} = \sigma_{0.2} \left[\frac{1 + \left(\frac{\sigma_{1.0}}{\sigma_{0.2}} - 1 \right) A^{\frac{1}{n_2}}}{1 + \left(\frac{\sigma_{0.2}}{E_0} \right) \left(\frac{E_0}{E_{0.2}} - 1 \right) \left(\frac{\sigma_{1.0}}{\sigma_{0.2}} - 1 \right) \left(\frac{A^{\frac{1}{n_2}}}{n_2 B_2} \right)} \right] \quad (25)$$

where

$$A = \frac{B_2}{0.008 + \left(\frac{\sigma_{0.2}}{E_0} \right) \left(\frac{\sigma_{1.0}}{\sigma_{0.2}} - 1 \right) \left(1 - \frac{E_0}{E_{0.2}} \right)} \quad (26)$$

$$B_2 = 0.018 + \left(\frac{\sigma_{0.2}}{E_0} \right) \left(\frac{E_0}{E_{0.2}} - 1 \right) \quad (27)$$

The strain $\varepsilon_{2.0}$ is expressed by the following equation given by Quach et al. [2]:

$$\varepsilon_{2.0} = \frac{\sigma_{2.0} - \sigma_{0.2}}{E_{0.2}} + \left[0.008 + (\sigma_{1.0} - \sigma_{0.2}) \left(\frac{1}{E_0} - \frac{1}{E_{0.2}} \right) \right] \left(\frac{\sigma_{2.0} - \sigma_{0.2}}{\sigma_{1.0} - \sigma_{0.2}} \right)^{n_2} + \varepsilon_{0.2} \quad (28)$$

In the third stage ($\varepsilon_{2.0} < \varepsilon_s \leq \varepsilon_{su}$), the stress is expressed as a function of strain as [3]:

$$\sigma_s = \frac{A_3 + B_3 \varepsilon_s}{1 + \varepsilon_s} \quad (29)$$

where

$$A_3 = \sigma_{2.0}(1 + \varepsilon_{2.0}) - B_3\varepsilon_{2.0} \quad (30)$$

$$B_3 = \frac{\sigma_{su}(1 + \varepsilon_{su}) - \sigma_{2.0}(1 + \varepsilon_{2.0})}{\varepsilon_{su} - \varepsilon_{2.0}} \quad (31)$$

where ε_{su} is the ultimate strain and σ_{su} is the ultimate stress.

The ultimate strain and stress are proposed by Quach et al. [2] as follows:

$$\sigma_{su} = \sigma_{ut}(1 + \varepsilon_{ut})^2 \quad (32)$$

$$\varepsilon_{su} = 1 - \frac{1}{1 + \varepsilon_{ut}} \quad (33)$$

where σ_{ut} and ε_{ut} are the ultimate tensile strength and ultimate tensile strain respectively and are given by

$$\sigma_{ut} = \sigma_{0.2} \left[\frac{1 - 0.0375(n - 5)}{0.2 + 185e} \right] \quad (34)$$

$$\varepsilon_{ut} = 1 - \frac{\sigma_{0.2}}{\sigma_{ut}} \quad (35)$$

2.4. Material model for confined concrete

The confinement provided by the steel tube on the concrete core in circular concrete-filled stainless steel or steel tubular columns is passive. The concrete expansion causes the elongation of the steel tube that induces compressive confining stresses on the concrete core. The confining pressure increases with increasing the axial strain. Madas and Elnashai [29]

proposed a passive confinement model for confined concrete in which the concrete confinement varies with the axial strain. They reported that the confinement model given by Mander et al. [30] overestimates the confining pressures on the concrete. Liang and Fragomeni [16] proposed a confining pressure model for concrete in circular CFST columns. The general stress–strain curve for confined concrete in circular CFST columns suggested by Liang and Fragomeni [16] is shown in Fig. 3.

The concrete stress from O to A on the stress–strain curve is calculated based on the equations given by Mander et al. [30] as

$$\sigma_c = \frac{f'_{cc} \lambda (\varepsilon_c / \varepsilon'_{cc})}{\lambda - 1 + (\varepsilon_c / \varepsilon'_{cc})^\lambda} \quad (36)$$

$$\lambda = \frac{E_c}{E_c - (f'_{cc} / \varepsilon'_{cc})} \quad (37)$$

$$E_c = 3320 \sqrt{\gamma_c f'_c} + 6900 \quad (\text{MPa}) \quad (38)$$

in which σ_c denotes the compressive concrete stress, f'_{cc} is the effective compressive strength of confined concrete, f'_c is the compressive strength of concrete cylinder, ε_c is the compressive concrete strain, ε'_{cc} is the strain at f'_{cc} , E_c is the Young's modulus of concrete given by ACI 318-11 [31], and γ_c is the strength reduction factor proposed by Liang [14] to account for the column section size effect, expressed by

$$\gamma_c = 1.85 D_c^{-0.135} \quad (0.85 \leq \gamma_c \leq 1.0) \quad (39)$$

where D_c is the diameter of the concrete core. The equation proposed by Mander et al. [30] for determining the compressive strength of confined concrete was modified by Liang and Fragomeni [16] using the strength reduction factor γ_c as follows:

$$f'_{cc} = \gamma_c f'_c + k_1 f_{rp} \quad (40)$$

$$\varepsilon'_{cc} = \varepsilon'_c \left(1 + k_2 \frac{f_{rp}}{\gamma_c f'_c} \right) \quad (41)$$

where f_{rp} is the lateral confining pressure on the concrete and k_1 and k_2 are taken as 4.1 and 20.5 respectively. The strain ε'_c is the strain at f'_c of the unconfined concrete, given by

$$\varepsilon'_c = \begin{cases} 0.002 & \text{for } \gamma_c f'_c \leq 28 \text{ (MPa)} \\ 0.002 + \frac{\gamma_c f'_c - 28}{54000} & \text{for } 28 < \gamma_c f'_c \leq 82 \text{ (MPa)} \\ 0.003 & \text{for } \gamma_c f'_c > 82 \text{ (MPa)} \end{cases} \quad (42)$$

Based on the work of Hu et al. [12] and Tang et al. [32], Liang and Fragomeni [16] proposed an accurate confining pressure model for normal and high strength concrete in circular CFST columns, which is adopted in the present numerical model as follows:

$$f_{rp} = \begin{cases} 0.7(v_e - v_s) \frac{2t}{D - 2t} \sigma_{0.2} & \text{for } \frac{D}{t} \leq 47 \\ \left(0.006241 - 0.0000357 \frac{D}{t} \right) \sigma_{0.2} & \text{for } 47 < \frac{D}{t} \leq 150 \end{cases} \quad (43)$$

in which D is the outer diameter and t is the thickness of the steel tube and ν_e and ν_s are Poisson's ratio of the steel tube with and without concrete infill, respectively. Tang et al. [32] suggested that Poisson's ratio ν_s is taken as 0.5 at the maximum strength point and ν_e is given by

$$\nu_e = 0.2312 + 0.3582\nu_e' - 0.1524\left(\frac{f_c'}{\sigma_{0.2}}\right) + 4.843\nu_e'\left(\frac{f_c'}{\sigma_{0.2}}\right) - 9.169\left(\frac{f_c'}{\sigma_{0.2}}\right)^2 \quad (44)$$

$$\nu_e' = 0.881 \times 10^{-6} \left(\frac{D}{t}\right)^3 - 2.58 \times 10^{-4} \left(\frac{D}{t}\right)^2 + 1.953 \times 10^{-2} \left(\frac{D}{t}\right) + 0.4011 \quad (45)$$

It is noted that the confining pressure model proposed by Liang and Fragomeni [16] can be used for concrete confined by high strength steel tubes with significant strain hardening and has been verified by experimental results [15, 27]. In addition, it has been used to simulate the behavior of confined concrete in circular CFSST columns with acceptable accuracy [22].

The parts AB and BC of the stress–strain curve shown in Fig. 3 can be described by

$$\sigma_c = \begin{cases} \beta_c f_{cc}' + \left(\frac{\varepsilon_{cu} - \varepsilon_c}{\varepsilon_{cu} - \varepsilon_{cc}'}\right) (f_{cc}' - \beta_c f_{cc}') & \text{for } \varepsilon_{cc}' < \varepsilon_c \leq \varepsilon_{cu} \\ \beta_c f_{cc}' & \text{for } \varepsilon_c > \varepsilon_{cu} \end{cases} \quad (46)$$

where ε_{cu} is taken as 0.02 as suggested by Liang and Fragomeni [16] based on the experimental results, and β_c is a factor accounting for the confinement effect by the stainless steel tube on the post-peak strength and ductility of the confined concrete, which is given by Hu et al. [12] as

$$\beta_c = \begin{cases} 1.0 & \text{for } \frac{D}{t} \leq 40 \\ 0.0000339 \left(\frac{D}{t} \right)^2 - 0.010085 \left(\frac{D}{t} \right) + 1.3491 & \text{for } 40 < \frac{D}{t} \leq 150 \end{cases} \quad (47)$$

2.5. Analysis procedure

In the nonlinear analysis, the axial load-strain curve for a CFSST short column is determined by gradually increasing the axial strain and computing the corresponding axial force (P), which is calculated as the stress resultant in the composite cross-section. When the axial load drops below a specified percentage of the maximum axial load (P_{\max}) such as $0.5P_{\max}$ or when the axial strain in concrete exceeds the specified ultimate strain ε_{cu} , the iterative analysis process can be stopped as discussed by Liang [14, 33]. The ultimate axial strength of a CFSST short column under axial compression is taken as the maximum axial load from its complete axial load-strain curve [33].

The analysis procedure for determining the axial load-strain curve for a CFSST short column under axial compression is given as follows [33]:

1. Input data.
2. Discretize the column cross-section into fiber elements.
3. Initialize fiber axial strains $\varepsilon = \Delta\varepsilon$.
4. Calculate fiber stresses using the material uniaxial stress-strain relationships.
5. Compute the axial force P as the stress resultant in the cross-section.
6. Increase the fiber axial strain by $\varepsilon = \varepsilon + \Delta\varepsilon$.
7. Repeat Steps 4 to 6 until $P < 0.5P_{\max}$ or $\varepsilon > \varepsilon_{cu}$.

The axial force acting on the composite section is determined as the stress resultant, which is expressed by

$$P = \sum_{i=1}^{ns} \sigma_{s,i} A_{s,i} + \sum_{j=1}^{nc} \sigma_{c,j} A_{c,j} \quad (48)$$

where P is the axial load, $\sigma_{s,i}$ is the longitudinal stress at the centroid of steel fiber i , $A_{s,i}$ is the area of steel fiber i , $\sigma_{c,j}$ is the longitudinal stress at the centroid of concrete fiber j , $A_{c,j}$ is the area of concrete fiber j , ns is the total number of steel fiber elements and nc is the total number of concrete fiber elements.

3. Validation of the fiber element model

3.1. Ultimate axial strengths

The ultimate axial strengths of circular CFSST short columns predicted by the fiber element model are compared with experimental results presented by Lam and Gardner [9] and Uy et al. [10]. Geometry and material properties of specimens are given in Table 1. The predicted and experimental ultimate axial strengths of circular CFSST columns under axial compression are also given in Table 1, where $P_{u.exp}$ is the experimental ultimate axial load and $P_{u.fib}$ is denoted as the ultimate axial load predicted by the fiber element model at the measured maximum axial strain (ε_{max}). It can be seen from Table 1 that the fiber element model generally gives good predictions of the ultimate axial strengths of circular CFSST short columns. The mean ultimate axial strength computed by the fiber element model is 97% of the experimental value. The standard deviation of $P_{u.fib}/P_{u.exp}$ is 0.08 while its coefficient of

variation is 0.09. The discrepancy between the predicted and experimental results is attributed to the uncertainty of the actual concrete compressive strength because the average concrete compressive strength was used in the fiber element analysis. It is noted that specimens shown in Table 1 include normal strength stainless steel tubes filled with normal strength concrete and normal strength stainless steel tubes filled with high strength concrete. Therefore, the proposed fiber element model can be used for the design and analysis of axially loaded CFSST columns made of normal and high strength concrete.

3.2. Axial load–strain curves

Fig. 4 shows the predicted and experimental axial load–strain curves for Specimen CHS 114 × 6-C30 tested by Lam and Gardner [9]. It appears that the fiber element model generally predicts well the experimental axial load–strain curve for the specimen. The predicted initial axial stiffness of the column is slightly higher than the experimental one. This is likely due to the uncertainty of the actual concrete stiffness and strength as the average concrete compressive strength was used in the fiber element analysis. However, it can be seen from Fig. 4 that the fiber element model accurately predicts the strain-hardening behavior of the specimen. The results obtained for Specimen CHS 114 × 6-C60 tested by Lam and Gardner [9] are presented in Fig. 5. The figure shows that the fiber element results are in good agreement with experimentally observed behavior. The initial axial stiffness of the column is well predicted, but the experimental axial load–strain curve differs from the computational one at the axial load higher than 1100 kN.

The predicted axial load–strain curve for Specimen C30-50×1.2A is compared with experimental one provided by Uy et al. [10] in Fig. 6. It can be observed that the fiber element

model closely predicts the initial axial stiffness of the specimen before attaining a loading level about 80 kN. After this loading, the axial stiffness of the specimen obtained from tests slightly differs from fiber element predictions. This is likely attributed to the uncertainty of the concrete stiffness and strength. Further comparison of axial load–strain curves for Specimen C20-100×1.6B tested by Uy et al. [10] is shown in Fig. 7. The figure demonstrates that these two curves are almost identical up to the loading level of about 350 kN. After that the experimental curve departs from computational one. The discrepancy is most likely due to the uncertainty of the actual concrete compressive strength and stiffness as the average concrete compressive strength was used in the analysis. The comparative studies demonstrate that the fiber element model yields good predictions of the behavior of circular CFSST short columns under axial compression.

4. Parametric study

The fiber element model developed was employed to investigate the effects of the diameter-to-thickness ratio, concrete compressive strength and stainless steel proof stress on the behavior of circular CFSST short columns under axial loading. Uy et al. [10] reported that CFSST short columns undergone large plastic deformations with significant strain hardening. The tests of CFSST short columns were stopped before failure occurred owing to the large plastic deformation. Tests indicated that CFSST short columns exhibited very good ductility and the axial strain of CFSST short columns under axial compression could be up to 0.2. Therefore, the ultimate axial strain (ϵ_{cu}) was taken as 0.2 in the following parametric study. For stress-strain curves without descending part, the ultimate axial strengths of CFSST short columns were taken as the axial load corresponding to the ultimate axial strain of 0.2. The Young's modulus of stainless steel was 200 GPa.

4.1. Evaluation of material constitutive models for stainless steels

The accuracy of full-range two-stage stress–strain curves proposed by Rasmussen [1] and three-stage stress–strain relationship presented by Abdella et al. [3] have been investigated using the present fiber element analysis program developed. Table 2 shows a comparison of the ultimate axial strengths of CFSST columns determined using these two material models for stainless steels. The material properties of these specimens can be found in Table 1. It can be seen from Table 2 that the two-stage stress–strain relationships proposed by Rasmussen [1] generally underestimate the ultimate axial strengths of circular CFSST columns. The mean ultimate axial strength computed by the fiber element model with two-stage curves is 81% of the experimental value. The standard deviation of $P_{u, fib1}/P_{u, exp}$ is 0.08 while its coefficient of variation is 0.10. The mean ultimate axial strength predicted using Abdella et al. [3] model is 97% of the experimental value. The standard deviation of $P_{u, fib}/P_{u, exp}$ is 0.08 and its coefficient of variation is 0.09. The evaluation demonstrates that the three-stage stress–strain relationships given by Abdella et al. [3] provide reliable results for circular CFSST columns under axial compression.

The accuracy of the constitutive models for stainless steels can be assessed by comparisons of predicted axial load–strain curves using the two-stage and three-stage stress–strain relationships. Fig. 8 presented a comparison of the axial load–strain curves computed by Rasmussen constitutive model [1] and Abdella et al. material model [3]. Close agreement between these two material models is achieved up to the proof stress of the stainless steel. However, there are significant differences between the axial load–strain curves obtained from both material models for the stress higher than the proof stress.

4.2. Effects of D/t ratio

The D/t ratio is one of the important variables affecting the behavior of circular CFSST short columns under axial compression. This is due to both the confinement effects and steel area varies with the D/t ratio. Column C7 given in Table 3 was analysed to examine the effects of D/t ratios. The typical D/t ratios of 32, 42 and 64 were considered by changing the thickness of the stainless steel tube while maintaining the same cross-section size.

Fig. 9 depicts the axial load–strain curves for circular CFSST columns with various D/t ratios. It appears that the ultimate axial load of circular CFSST columns decreases with increasing the D/t ratio. When increasing the D/t ratio from 32 to 42 and 64, the ultimate axial strength of the short column decreases by 17% and 44%, respectively. In addition, the circular CFSST column exhibits strain hardening behavior when the D/t ratio is small. This is due to both the steel area and confinement effect increases with decreasing the D/t ratio. More importantly, the ductility of circular CFSST short columns increases with decreasing the D/t ratio. Similar conclusion was observed by Uy et al. [10] in their experimental research on circular CFSST short columns under axial loading. The ductility of a structural member or section is defined by Liang [14] as the ability to undergo large plastic deformation without significant strength degradation.

4.3. Effects of concrete compressive strengths

It is important to understand the effects of concrete compressive strengths on the stiffness and ductility of circular CFSST short columns under axial loading. Columns C13, C14 and C15

given in Table 3 were analysed again to investigate the effects of the concrete compressive strengths on the behavior of circular CFSST columns.

Fig. 10 shows the axial load–strain curves for the circular CFSST columns filled with concrete of different compressive strengths. The ultimate axial strength and stiffness of circular CFSST columns are found to increase with increasing the concrete compressive strength. Increasing the concrete compressive strength from 70 MPa to 90 MPa and 110 MPa increases the ultimate axial strength by 10% and 20%, respectively. It can also be seen from Fig. 10 that increasing the concrete compressive strength results in a slight increase in the initial stiffness of the column. Despite of the use of high strength concrete, these circular CFSST short columns exhibit good ductility, which is the ability to undergo large plastic deformation without significant strength degradation.

4.4. Effects of stainless steel strengths

The numerical model developed was utilised to investigate the effects of the proof stress of stainless steel on the compressive behavior of circular CFSST columns. Column C36 given in Table 3 was analysed to examine the effects of proof stress on the behavior of CFSST columns. Austenitic and duplex stainless steel tubes with proof stresses of 240 MPa and 530 MPa and non-linearity index of 7 and 5 were considered.

The axial load–strain curves for the circular CFSST columns made of different strength stainless steel tubes are presented in Fig. 11. It can be observed from the figure that increasing the proof stress of the stainless steel noticeably increases the ultimate axial loads of circular CFSST columns. When increasing the proof stress of the stainless steel from 240 MPa to 530

MPa, the ultimate axial strength of the column increases by 31%. Computational results indicate that the proof stress of stainless steel does not have an effect on the initial axial stiffness of the columns.

5. Design models

5.1. ACI-318 codes

The design equation given in ACI-318 [31] codes does not account for the concrete confinement effects on the ultimate axial strength of composite columns, which is expressed by

$$P_{u,ACI} = A_s f_{sy} + 0.85 A_c f_c \quad (49)$$

where A_c is the cross-sectional area of the concrete core, A_s is the cross-sectional area of steel tube, f_{sy} is the steel yield strength which is taken as 0.2% proof stress for stainless steels.

5.2. Eurocode 4

The ultimate axial loads of circular CFSST columns were compared with the design strengths predicted by the Eurocode 4 [34]. The code takes into account the concrete confinement effect by the circular steel tube. The EC4 equation for ultimate axial strength of a CFST column is given as

$$P_{u.EC4} = \eta_a A_s f_{sy} + A_c f_c \left(1 + \eta_c \frac{t}{D} \frac{f_{sy}}{f_c} \right) \quad (50)$$

where $\eta_a = 0.25(3 + 2\bar{\lambda}) \leq 1.0$, $\eta_c = 4.9 - 18.5\bar{\lambda} + 17\bar{\lambda}^2 \geq 1.0$, in which $\bar{\lambda}$ is the relative slenderness of a CFSST column, calculated as

$$\bar{\lambda} = \sqrt{\frac{N_{pl.Rk}}{N_{cr}}} \quad (51)$$

where $N_{pl.Rk}$ is the cross-section plastic resistance of the CFSST column, given by

$$N_{pl.Rk} = A_s \sigma_{0.2} + A_c f_c \quad (52)$$

In Eq. (51), N_{cr} is the Euler buckling load of the pin-ended CFSST column and expressed by

$$N_{cr} = \frac{\pi^2 (EI)_{eff}}{L^2} \quad (53)$$

where $(EI)_{eff}$ is the effective flexural stiffness of a CFSST section, given as

$$(EI)_{eff} = E_s I_s + 0.6 E_{cm} I_c \quad (54)$$

In Eq. (53), L is the effective length of the CFSST column.

5.3. The proposed design model based on Liang and Fragomeni's formula

The ultimate axial strength of a CFSST short column under axial compression is influenced by confinement of the concrete core. A design model for determining the ultimate axial strength of a CFSST short column with confinement effects was proposed by Liang and Fragomeni [16] as follows:

$$P_{u.design} = (\gamma_c f'_c + 4.1 f_{rp}) A_c + \gamma_s \sigma_{0.2} A_s \quad (51)$$

where γ_c is calculated using Eq. (39), f_{rp} is given by Eq. (43), and γ_s is the strength factor for the stainless steel tube, which is proposed as follows:

$$\gamma_s = \begin{cases} 3 \left(\frac{D}{t} \right)^{-0.1} & \text{for } \frac{D}{t} < 80 \\ 2 \left(\frac{D}{t} \right)^{-0.1} & \text{for } \frac{D}{t} \geq 80 \end{cases} \quad (52)$$

5.4. Comparisons of design models

The fiber element model was utilized to analyze CFSST columns in order to develop a design model. The geometric and material properties used in the nonlinear regression analysis are given in Table 3. It should be noted that columns are selected with a wide range of diameter-to-thickness ratio ranging from 20 to 100. The stainless steel tubes were filled with normal and high strength concrete with compressive strengths ranging from 30 MPa to 110 MPa. The ultimate axial strengths of circular CFSST columns calculated using Eq. (51) are compared with numerical results in Table 3, where $P_{u.design}$ is the ultimate axial strength calculated using Eq. (51). It can be seen from the table that the proposed design formula gives very good predictions of the ultimate axial strengths of

circular CFSST columns except for Columns C26, C41, C42, C46 and C51. The ultimate axial strengths obtained from the fiber element model for these columns are governed by the strain hardening of stainless steel. The mean ultimate axial strength predicted by Eq. (51) is 97% of the numerical value. The standard deviation of $P_{u.design}/P_{u.num}$ is 0.05 while its coefficient of variation is also 0.06. Therefore, it can be concluded that the proposed design formula can be used in the design of axially loaded circular CFSST columns made of normal and high strength concrete and stainless steel tubes with D/t ratios ranging from 20 to 100.

The ultimate axial strengths for axially loaded CFSST columns predicted by the proposed design model and design codes are compared with the experimental results in Table 4. It can be observed that the ultimate axial strengths calculated by the proposed design model agrees well with experimental results. However, existing design codes ACI-318 [31] and Eurocode 4 [34] give conservative predictions of the ultimate axial strengths of CFSST columns. The mean ultimate axial strength calculated using the proposed design model is 99% of the experimental value. The standard deviation of $P_{u.design}/P_{u.exp}$ is 0.11 while its coefficient of variation is 0.11. The mean ultimate axial strength predicted using ACI-318 codes is 54% of the experimental value. The standard deviation of $P_{u.ACI}/P_{u.exp}$ is 0.09 and its coefficient of variation is 0.17. The mean ultimate axial strength predicted using Eurocode 4 is 78% of the experimental value. The standard deviation of $P_{u.EC4}/P_{u.exp}$ is 0.11 and its coefficient of variation is 0.14.

6. Conclusions

A fiber element model incorporating the full-range three-stage stress–strain relationships for stainless steel has been presented in this paper for the nonlinear analysis of circular CFSST short columns under axial compression. The comparative studies performed show that the

three-stage material constitutive model for stainless steels gives more accurate predictions of the experimentally observed behavior of CFSST short columns than the two-stage material model. It is demonstrated that the developed fiber element model considering concrete confinement effects predicts well the load–strain behavior and ultimate axial strengths of CFSST short columns tested by independent researchers. The proposed design model for axially loaded CFSST short columns is verified by experimental and numerical results. It is found that the design method given in ACI-318 codes [31] is highly conservative for estimating the ultimate axial strengths of circular CFSST short columns because the codes do not account for the concrete confinement effects and significant strain hardening of stainless steels in compression. Eurocode 4 [34] considers the effects of concrete confinement in the calculation of the ultimate axial strength of circular concrete-filled steel columns. However, it still provides conservative design strengths since the significant strain hardening of stainless steel has not been taken into account in Eurocode 4. The confining pressure model proposed by Liang and Fragomeni [16] gives conservative predictions of the confinement in CFSST columns. Further research is needed to develop an accurate passive confinement model for concrete in circular CFSST columns to account for the effects of significant strain hardening of stainless steel tubes on the confinement.

References

- [1] Rasmussen KJR. Full-range stress–strain curves for stainless steel alloys. *J Constr Steel Res* 2003;59(1):47-61.
- [2] Quach WM, Teng JG, Chung KF. Three-stage full-range stress–strain model for stainless steels. *J Struct Eng ASCE* 2008;134(9):1518-27.

- [3] Abdella K, Thannon RA, Mehri AI, Alshaikh FA. Inversion of three-stage stress–strain relation for stainless steel in tension and compression. *J Constr Steel Res* 2011;67(5):826-32.
- [4] Schneider SP. Axially loaded concrete-filled steel tubes. *J Struct Eng ASCE* 1998;124(10):1125-38.
- [5] O’Shea MD, Bridge RQ. Design of circular thin-walled concrete filled steel tubes. *J Struct Eng ASCE* 2000;126(11):1295-1303.
- [6] Giakoumelis G, Lam D. Axial capacity of circular concrete-filled tube columns. *J Constr Steel Res* 2004;60(7):1049-68.
- [7] Sakino K, Nakashara H, Morino S, Nishiyama I. Behavior of centrally loaded concrete-filled steel-tube short columns. *J Struct Eng ASCE* 2004;130(2):180-188.
- [8] Young B, Ellobody E. Experimental investigation of concrete-filled cold-formed high strength stainless steel tube columns. *J Constr Steel Res* 2006;62(5):484-92.
- [9] Lam D, Gardner L. Structural design of stainless steel concrete filled columns. *J Constr Steel Res* 2008;64(11):1275-82.
- [10] Uy B, Tao Z, Han LH. Behaviour of short and slender concrete-filled stainless steel tubular columns. *J Constr Steel Res* 2011;67(3):360-78.
- [11] Lakshmi B. Shanmugam NE. Nonlinear analysis of in-filled steel-concrete composite columns. *J Struct Eng ASCE* 2002;128(7):922-33.
- [12] Hu HT, Huang CS, Chen ZL. Finite element analysis of CFT columns subjected to an axial compressive force and bending moment in combination. *J Constr Steel Res* 2005;61(12):1692-1712.
- [13] Hatzigeorgiou GD. Numerical model for the behavior and capacity of circular CFT columns, Part I: Theory. *Eng Struct* 2008;30(6):1573-78.

- [14] Liang QQ. Performance-based analysis of concrete-filled steel tubular beam-columns, Part I: Theory and algorithms. *J Constr Steel Res* 2009;65(2):363-72.
- [15] Liang QQ. Performance-based analysis of concrete-filled steel tubular beam-columns, Part II: Verification and applications. *J Constr Steel Res* 2009;65(2):351-62.
- [16] Liang QQ, Fragomeni S. Nonlinear analysis of circular concrete-filled steel tubular short columns under axial loading. *J Constr Steel Res* 2009;65(12):2186-96.
- [17] Choi KK, Xiao Y. Analytical studies of concrete-filled circular steel tubes under axial compression. *J Struct Eng ASCE* 2010;136(5):565-73.
- [18] Tao Z, Wang ZB, Yu Q. Finite element modelling of concrete-filled steel stub columns under axial compression. *J Constr Steel Res* 2013;89:121-31.
- [19] Ellobody E. A consistent nonlinear approach for analysing steel, cold-formed steel, stainless steel and composite columns at ambient and fire conditions. *Thin Wall Struct* 2013;68:1-17.
- [20] Ellobody E, Young, B. Design and behavior of concrete-filled cold-formed stainless steel tube columns. *Eng Struct* 2006;28(5):716-28.
- [21] Tao Z, Uy B, Liao FY, Han LH, Nonlinear analysis of concrete-filled square stainless steel stub columns under axial compression. *J Constr Steel Res* 2011;67(11):1719-32.
- [22] Hassanein MF, Kharoob OF, Liang QQ. Behaviour of circular concrete-filled lean duplex stainless steel tubular short columns. *Thin Wall Struct* 2013;68:113-123.
- [23] El-Tawil S, Sanz-picón CF, Deierlein GG. Evaluation of ACI 318 and AISC (LRFD) strength provisions for composite beam-columns. *J Constr Steel Res* 1995;34(1):103-26.
- [24] Hajjar JF, Gourley BC. Representation of concrete-filled steel tube cross-section strength. *J Struct Eng ASCE* 1996;122(11):1327-36.
- [25] Shanmugam NS, Lakshmi B, Uy B. An analytical model for thin-walled steel box columns with concrete in-fill. *Eng Struct* 2002;24(6):825-38.

- [26] Liang QQ. High strength circular concrete-filled steel tubular slender beam-columns, Part I: Numerical analysis. *J Constr Steel Res*, 2011; 67(2):164-171.
- [27] Liang QQ. High strength circular concrete-filled steel tubular slender beam-columns, Part II: Fundamental behavior. *J Constr Steel Res*, 2011; 67(2): 172-180.
- [28] Ramberg W, Osgood WR. Description of stress–strain relations from offset yield strength values. NACA Technical Note no. 927, 1944.
- [29] Madas P, Elnashai AS. A new passive confinement model for the analysis of concrete structures subjected to cyclic and transient dynamic loading. *Earthquake Eng and Struct Dyn* 1992; 21(5):409-431.
- [30] Mander JB, Priestly MNJ, Park R. Theoretical stress–strain model for confined concrete. *J Struct Eng ASCE* 1988;114(8):1804-26.
- [31] ACI-318-11. Building code requirements for structural concrete and commentary ACI Committee 318, Detroit (MI) 2011.
- [32] Tang J, Hino S, Kuroda I, Ohta T. Modeling of stress–strain relationships for steel and concrete in concrete filled circular steel tubular columns. *Steel Constr Eng JSSC* 1996; 3(11):35-46.
- [33] Liang QQ. Analysis and design of steel and composite structures. London and New York: CRC Press, Taylor and Francis Group, 2014.
- [34] Eurocode 4 (1994), Design of composite steel and concrete structures, Part 1.1, General rules and rules for buildings, DD ENV 1994-1-1, London, United Kingdom.

Figures and tables

Table 1 Ultimate axial loads of circular CFSST short columns.

Specimens	D (mm)	t (mm)	D/t	L (mm)	$\sigma_{0.2}$ (MPa)	E_0 (GPa)	n	f'_c (MPa)	ε_{max}	$P_{u.exp}$ (kN)	$P_{u.fib}$ (kN)	$\frac{P_{u.fib}}{P_{u.exp}}$	Ref.
CHS 104 × 2-C30	104	2	52	300	412	191.9	4.3	31	0.078	699	715.51	1.02	[9]
CHS 104 × 2-C60	104	2	52	300	412	191.9	4.3	49	0.095	901	871.37	0.97	
CHS 104 × 2-C100	104	2	52	300	412	191.9	4.3	65	0.044	1133	903.18	0.80	
CHS 114 × 6-C30	114.3	6.02	19	300	266	183.6	8.4	31	0.110	1424	1452.75	1.02	
CHS 114 × 6-C60	114.3	6.02	19	300	266	183.6	8.4	49	0.163	1648	1859.24	1.13	
CHS 114 × 6-C100	114.3	6.02	19	300	266	183.6	8.4	65	0.021	1674	1369.65	0.82	
C20-50 × 1.2A	50.8	1.2	42	150	291	195	7	20	0.178	192	194.01	1.01	[10]
C20-50 × 1.2B	50.8	1.2	42	150	291	195	7	20	0.149	164	179.47	1.09	
C30-50 × 1.2A	50.8	1.2	42	150	291	195	7	30	0.160	225	208.88	0.93	
C20-50 × 1.6A	50.8	1.6	32	150	298	195	7	20	0.139	203	218.64	1.08	
C20-50 × 1.6B	50.8	1.6	32	150	298	195	7	20	0.138	222	218.01	0.98	
C30-50 × 1.6A	50.8	1.6	32	150	298	195	7	30	0.177	260	268.85	1.03	
C30-50 × 1.6B	50.8	1.6	32	150	298	195	7	30	0.179	280	270.23	0.97	
C20-100 × 1.6A	101.6	1.6	64	300	320	195	7	20	0.191	637	575.98	0.90	
C20-100 × 1.6B	101.6	1.6	64	300	320	195	7	20	0.206	675	598.49	0.89	
C30-100 × 1.6A	101.6	1.6	64	300	320	195	7	30	0.154	602	587.98	0.98	
C30-100 × 1.6B	101.6	1.6	64	300	320	195	7	30	0.163	609	600.14	0.99	
Mean												0.97	
Standard deviation (SD)												0.08	
Coefficient of variation (COV)												0.09	

Table 2 Comparison of ultimate axial strengths of circular CFSST short columns.

Specimens	$P_{u.exp}$ (kN)	Rasmussen's model		Abdella et al. model	
		$P_{u.fib1}$ (kN)	$\frac{P_{u.fib1}}{P_{u.exp}}$	$P_{u.fib}$ (kN)	$\frac{P_{u.fib}}{P_{u.exp}}$
CHS 104 × 2-C30	699	640.27	0.92	715.51	1.02
CHS 104 × 2-C60	901	776.02	0.86	871.37	0.97
CHS 104 × 2-C100	1133	864.15	0.76	903.18	0.80
CHS 114 × 6-C30	1424	1282.65	0.90	1452.75	1.02
CHS 114 × 6-C60	1648	1507.86	0.91	1859.24	1.13
CHS 114 × 6-C100	1674	1376.66	0.82	1369.65	0.82
C20-50 × 1.2A	192	148.21	0.77	194.01	1.01
C20-50 × 1.2B	164	145.59	0.89	179.47	1.09
C30-50 × 1.2A	225	170.72	0.76	208.88	0.93
C20-50 × 1.6A	203	178.43	0.88	218.64	1.08
C20-50 × 1.6B	222	178.43	0.80	218.01	0.98
C30-50 × 1.6A	260	208.24	0.80	268.85	1.03
C30-50 × 1.6B	280	208.49	0.74	270.23	0.97
C20-100 × 1.6A	637	431.97	0.68	575.98	0.90
C20-100 × 1.6B	675	433.48	0.64	598.49	0.89
C30-100 × 1.6A	602	486.94	0.81	587.98	0.98
C30-100 × 1.6B	609	489.45	0.80	600.14	0.99
Mean			0.81		0.97
Standard deviation (SD)			0.08		0.08
Coefficient of variation (COV)			0.10		0.09

Table 3 Comparison of ultimate axial strengths of CFSST columns determined by numerical model and design model.

Specimens	D (mm)	t (mm)	D/t	$\sigma_{0.2}$ (MPa)	n	f'_c (MPa)	$P_{u.num}$ (kN)	$P_{u.design}$ (kN)	$\frac{P_{u.design}}{P_{u.num}}$
C1	50	2.63	19	530	5	30	547	546	1.00
C2	50	2.63	19	530	5	50	598	597	1.00
C3	50	2.63	19	530	5	70	641	640	1.00
C4	50	2.63	19	530	5	90	676	675	1.00
C5	50	2.63	19	530	5	110	705	704	1.00
C6	100	3.13	32	530	5	30	1473	1413	0.96
C7	100	3.13	32	530	5	50	1672	1612	0.96
C8	100	3.13	32	530	5	70	1852	1792	0.97
C9	100	3.13	32	530	5	90	2014	1955	0.97
C10	100	3.13	32	530	5	110	2158	2098	0.97
C11	50	1.19	42	530	5	30	298	283	0.95
C12	50	1.19	42	530	5	50	346	331	0.96
C13	50	1.19	42	530	5	70	390	376	0.96
C14	50	1.19	42	530	5	90	431	417	0.97
C15	50	1.19	42	530	5	110	468	455	0.97
C16	100	2.38	42	530	5	30	1194	1131	0.95
C17	100	2.38	42	530	5	50	1384	1324	0.96
C18	100	2.38	42	530	5	70	1561	1504	0.96
C19	100	2.38	42	530	5	90	1724	1669	0.97
C20	100	2.38	42	530	5	110	1872	1820	0.97
C21	100	1.92	52	530	5	30	965	920	0.95
C22	100	1.92	52	530	5	50	1098	1065	0.97
C23	100	1.92	52	530	5	70	1230	1210	0.98
C24	100	1.92	52	530	5	90	1363	1356	0.99
C25	100	1.92	52	530	5	110	1496	1501	1.00
C26	114	2.19	52	320	7	30	966	830	0.86
C27	114	2.19	52	320	7	50	1136	1015	0.89

C28	114	2.19	52	320	7	70	1305	1200	0.92
C29	114	2.19	52	320	7	90	1475	1385	0.94
C30	114	2.19	52	320	7	110	1645	1570	0.95
C31	114	1.78	64	320	7	30	819	729	0.89
C32	114	1.78	64	320	7	50	977	917	0.94
C33	114	1.78	64	320	7	70	1135	1104	0.97
C34	114	1.78	64	320	7	90	1294	1292	1.00
C35	114	1.78	64	320	7	110	1452	1480	1.02
C36	114	1.78	64	530	5	30	1051	1022	0.97
C37	114	1.78	64	530	5	50	1210	1210	1.00
C38	114	1.78	64	530	5	70	1368	1398	1.02
C39	114	1.78	64	530	5	90	1526	1586	1.04
C40	114	1.78	64	530	5	110	1684	1774	1.05
C41	114	1.43	80	320	7	30	685	537	0.78
C42	114	1.43	80	320	7	50	829	727	0.88
C43	114	1.43	80	320	7	70	974	917	0.94
C44	114	1.43	80	320	7	90	1118	1107	0.99
C45	114	1.43	80	320	7	110	1263	1297	1.03
C46	114	1.27	90	320	7	30	620	509	0.82
C47	114	1.27	90	320	7	50	757	700	0.92
C48	114	1.27	90	320	7	70	894	891	1.00
C49	114	1.27	90	320	7	90	1043	1082	1.04
C50	114	1.27	90	320	7	110	1233	1273	1.03
C51	114	1.14	100	320	7	30	567	485	0.86
C52	114	1.14	100	320	7	50	697	677	0.97
C53	114	1.14	100	320	7	70	835	869	1.04
C54	114	1.14	100	320	7	90	1027	1061	1.03
C55	114	1.14	100	320	7	110	1219	1253	1.02
Mean									0.97
Standard deviation (SD)									0.05
Coefficient of variation (COV)									0.06

Table 4 Comparison of ultimate axial strengths of CFSST columns determined by experiment, design codes and design model.

Specimens	D/t	$P_{u.exp}$ (kN)	ACI code		EC4 code		Design model	
			$P_{u.ACI}$ (kN)	$\frac{P_{u.ACI}}{P_{u.exp}}$	$P_{u.EC4}$ (kN)	$\frac{P_{u.exp}}{P_{u.EC4}}$	$P_{u.design}$	$\frac{P_{u.design}}{P_{u.exp}}$
CHS 104 × 2-C30	52	699	471	0.67	683	0.98	834	1.19
CHS 104 × 2-C60	52	901	591	0.66	818	0.91	974	1.08
CHS 104 × 2-C100	52	1133	698	0.62	939	0.83	1099	0.97
CHS 114 × 6-C30	19	1424	761	0.53	1138	0.80	1632	1.02
CHS 114 × 6-C60	19	1648	887	0.54	1279	0.78	1800	1.09
CHS 114 × 6-C100	19	1674	998	0.60	1405	0.84	1898	1.13
C20-50 × 1.2A	42	192	86	0.45	129	0.67	173	0.90
C20-50 × 1.2B	42	164	86	0.52	129	0.78	173	1.06
C30-50 × 1.2A	42	225	101	0.45	146	0.65	199	0.89
C20-50 × 1.6A	32	203	104	0.51	158	0.78	220	1.08
C20-50 × 1.6B	32	222	104	0.47	158	0.71	220	0.99
C30-50 × 1.6A	32	260	119	0.46	175	0.67	247	0.95
C30-50 × 1.6B	32	280	119	0.43	175	0.63	247	0.88
C20-100 × 1.6A	64	637	290	0.46	426	0.67	532	0.84
C20-100 × 1.6B	64	675	290	0.43	426	0.63	532	0.79
C30-100 × 1.6A	64	602	355	0.59	499	0.83	608	1.01
C30-100 × 1.6B	64	609	355	0.58	499	0.82	608	1.00
Mean				0.54		0.78		0.99
Standard deviation (SD)				0.09		0.11		0.11
Coefficient of variation (COV)				0.17		0.14		0.11

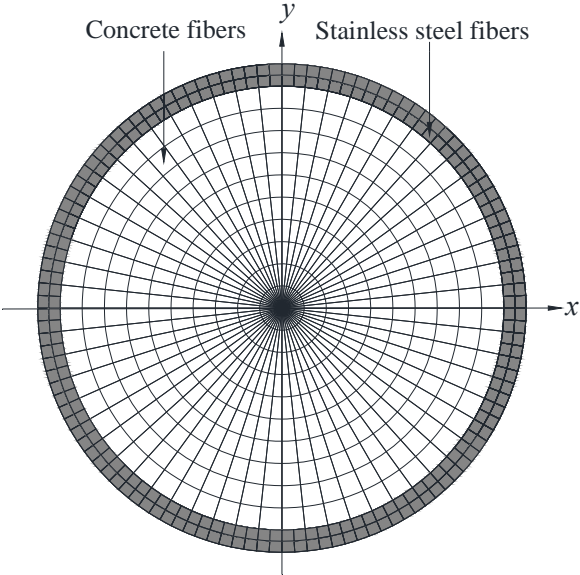


Fig. 1. Fiber element discretization of circular CFSST section.

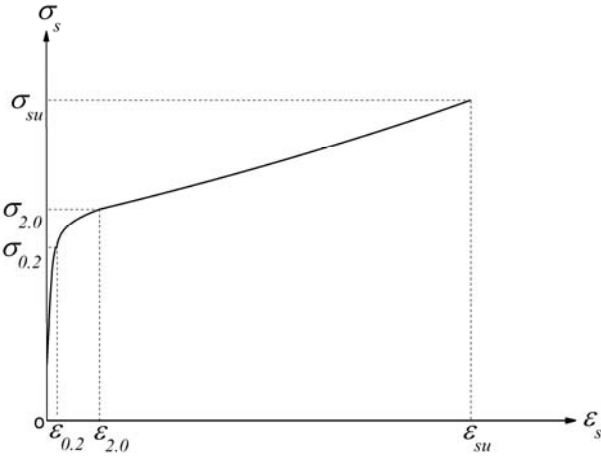


Fig. 2. Stress–strain curves for stainless steels in compression.

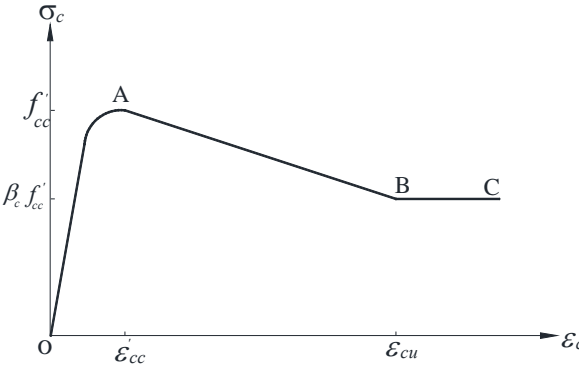


Fig. 3. Stress–strain curve for confined concrete in circular CFSST columns

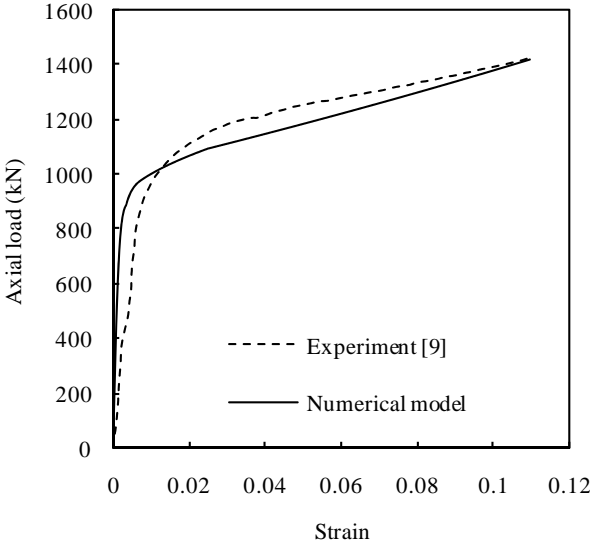


Fig. 4. Comparison of predicted and experimental axial load–strain curves for Specimen CHS 114 × 6-C30.

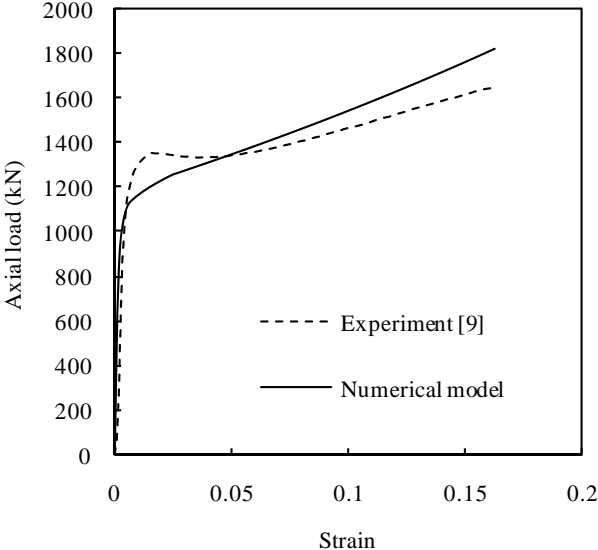


Fig. 5. Comparison of predicted and experimental axial load–strain curves for Specimen CHS 114 × 6-C60.

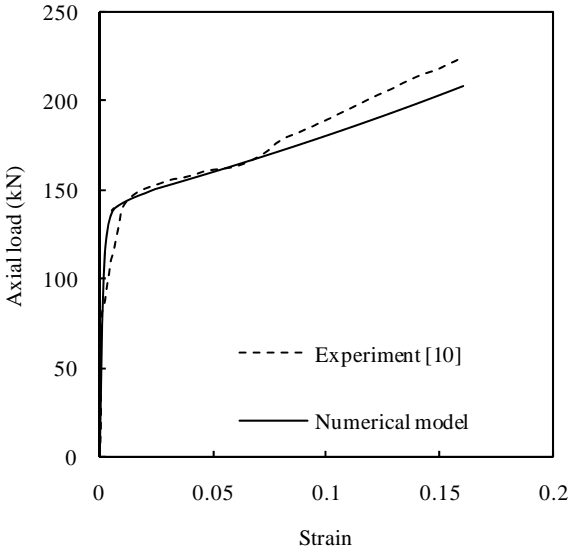


Fig. 6. Comparison of predicted and experimental axial load–strain curves for Specimen C30-50 × 1.2A.

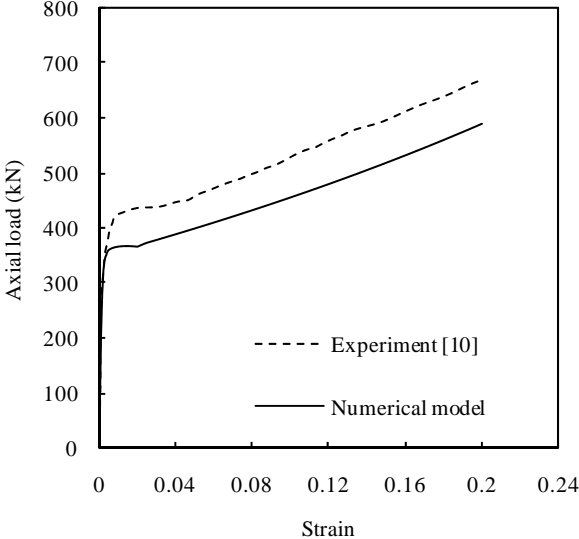


Fig. 7. Comparison of predicted and experimental axial load–strain curves for Specimen C20-100 × 1.6B.

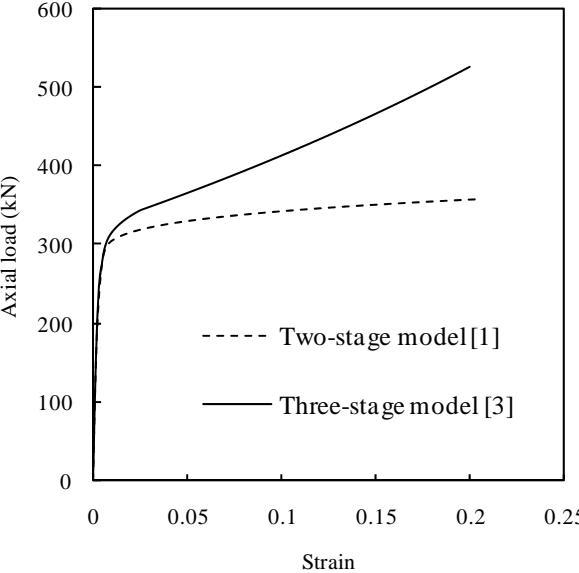


Fig. 8. Comparisons of two-stage and three-stage constitutive model for Specimen C1.

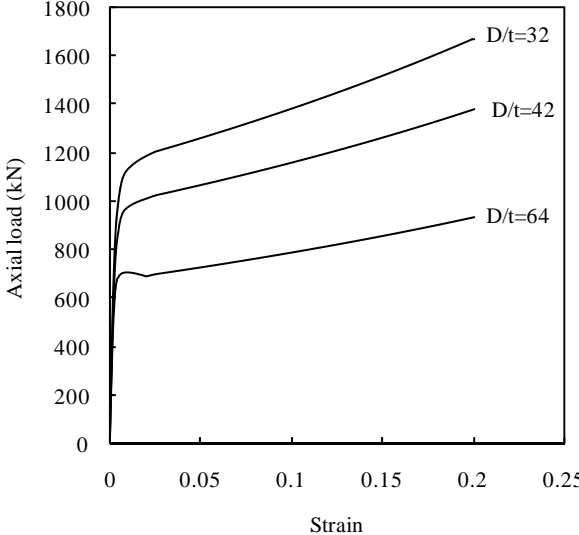


Fig. 9. Effects of D/t ratio on the axial load–strain behaviour of circular CFSST columns.

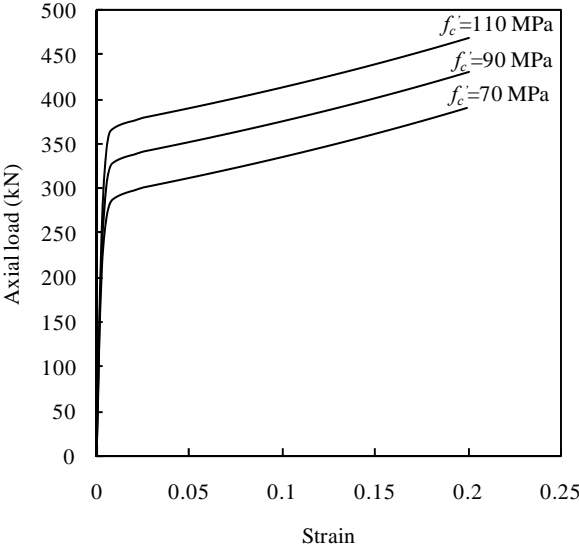


Fig. 10. Effects of concrete compressive strengths on axial load–strain curves for circular CFSST columns.

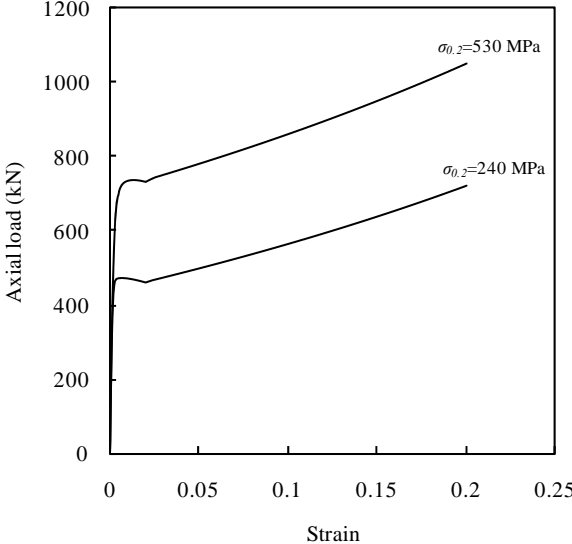


Fig. 11. Effects of stainless steel strengths on axial load–strain curves for circular CFSST columns.